geology and impact physics. Recent work has suggested that S-type asteroids with 'fresh' surfaces may have spectra that resemble (or trend towards) ordinary chondrite spectra (see, for example, ref. 21). Because Karin cluster asteroids are S-type[22] and have probably experienced minimal space weathering[23], we believe they could be used to examine this possibility. It would also be useful to compare the spectra of various Karin cluster asteroids, all of which should share the same age (that is, 5.8 Myr). Similarities and differences might help us to determine the rate of space weathering among S-type main-belt asteroids, and whether spectral alterations by space weathering are a function of time alone or are also dependent on asteroid size. Moreover, if the surfaces of the Karin-cluster members were given fresh surfaces by impact 5.8 Myr ago, the craters formed since that time by hypervelocity impacts may be used to infer the current crater production rate in the main belt, and the unknown shape of the main-belt's size distribution at small asteroid sizes.

It is possible that the Karin cluster may be the source of some asteroidal material evolving towards Earth. For example, we believe that impacts on Karin cluster asteroids could be the source of the zodiacal dust β-band discovered by the IRAS satellite[24]. We base this idea on two pieces of evidence: (1) the Karin cluster and the model-derived source of the β-band both have mean inclinations near 2.1°, and (2) the narrow inclination span of the β-band source ($\Delta i \approx 0.09°$) is analogous to that of our compact 39-body cluster ($\Delta i \approx 0.08°$)[25]. (The inclination span of the Koronis family, which has generally been taken as the source of the β-band, is $\Delta i \approx 0.45°$). As a second example, we believe the Karin breakup event could have produced some meteorites. These putative objects would need to have compositions consistent with S-type asteroids and cosmic-ray exposure[26] ages $\lesssim 5.8$ Myr. □

Methods

Hierarchical clustering method

The hierarchical clustering method (HCM) starts with an individual asteroid position in the proper elements space, and identifies bodies in its neighbourhood with mutual distances less than a threshold limit (d_{cutoff}). We define the distance in the (a_P, e_P, i_P) space by:

$$d = n a_P \sqrt{C_a(\delta a_P/a_P)^2 + C_e(\delta e_P)^2 + C_i(\delta \sin i_P)^2} \quad (1)$$

where $n a_P$ is the heliocentric velocity of an asteroid on a circular orbit having the semimajor axis a_P. $\delta a_P = |a_P^{(1)} - a_P^{(2)}|$, $\delta e_P = |e_P^{(1)} - e_P^{(2)}|$, and $\delta \sin i_P = |\sin i_P^{(1)} - \sin i_P^{(2)}|$. The indices (1) and (2) denote the two bodies under consideration. C_a, C_e and C_i are constants: we use $C_a = 5/4$, $C_e = 2$ and $C_i = 2$ (ref. 10). Other choices of these constants found in the literature yield similar results.

Statistical significance of the 39-body cluster

To demonstrate the >99% statistical significance of the 39-body cluster, we generated 100 synthetic orbital distributions corresponding to the Koronis family determined at $d_{cutoff} = 60$ m s^{-1} (that is, 1,500 asteroid positions at $2.83 < a_P < 2.95$ AU, $0.04 < e_P < 0.06$ and $0.033 < i_P < 0.04$), and applied our HCM algorithm to these data. Applying $d_{cutoff} = 10$ m s^{-1}, we were unable to find a cluster containing more than five members. We also used the HCM algorithm on 100 computer-generated asteroid belts (that is, 66,000 random orbital positions at $2.1 < a_P < 3.25$ AU, $e_P < 0.3$ and $i_P < 0.3$). Once again, $d_{cutoff} = 10$ m s^{-1} yielded no meaningful structures.

1. Durda, D. D., Greenberg, R. & Jedicke, R. Collisional models and scaling laws: a new interpretation of the shape of the main-belt asteroid size distribution. *Icarus* **135**, 431–440 (1998).
2. Michel, P., Benz, W., Tanga, P. & Richardson, D. C. Collisions and gravitational reaccumulation: Forming asteroid families and satellites. *Science* **294**, 1696–1700 (2001).
3. Zappalà, V., Cellino, A., Dell'Oro, A. & Paolicchi, P. in *Asteroids III* (eds Bottke, W. F., Cellino, A., Paolicchi, P. & Binzel, R.) (Univ. Arizona Press, in the press).
4. Chambers, J. E. & Wetherill, G. W. Making the terrestrial planets: N-body integrations of planetary embryos in three dimensions. *Icarus* **136**, 304–327 (1998).
5. Canup, R. M. & Asphaug, E. Origin of the Moon in a giant impact near the end of the Earth's formation. *Nature* **412**, 708–712 (2001).
6. Marzari, F., Davis, D. & Vanzani, V. Collisional evolution of asteroid families. *Icarus* **113**, 168–187 (1995).
7. Bottke, W. F., Vokrouhlický, D., Brož, M., Nesvorný, D. & Morbidelli, A. Dynamical spreading of asteroid families by the Yarkovsky effect. *Science* **294**, 1693–1696 (2001).
8. Benz, W. & Asphaug, E. Catastrophic disruptions revisited. *Icarus* **142**, 5–20 (1999).
9. Hirayama, K. Groups of asteroids probably of common origin. *Astron. J.* **31**, 185–188 (1918).
10. Zappalà, V., Cellino, A., Farinella, P. & Milani, A. Asteroid families. II. Extension to unnumbered multiopposition asteroids. *Astron. J.* **107**, 772–801 (1994).
11. Milani, A. & Knežević, Z. Asteroid proper elements and the dynamical structure of the asteroid main belt. *Icarus* **107**, 219–254 (1994).
12. Milani, A. & Farinella, P. The age of the Veritas asteroid family deduced by chaotic chronology. *Nature* **370**, 40–41 (1994).
13. Nesvorný, D., Morbidelli, A., Vokrouhlický, D., Bottke, W. F. & Brož, M. The Flora family: a case of the dynamically dispersed collisional swarm? *Icarus* **157**, 155–172 (2002).
14. *Asteroids Dynamic Site* 〈http://hamilton.dm.unipi.it/cgi-bin/astdys/astibo〉 (7 May 2002).
15. Morbidelli, A., Zappalà, A., Moons, M., Cellino, A. & Gonczi, R. Asteroid families close to mean motion resonances: Dynamical effect and physical implications. *Icarus* **118**, 132–154 (1995).
16. *IAU: Minor Planet Centre* 〈http://cfa-www.harvard.edu/cfa/ps/mpc.html〉 (7 May 2002).
17. Levison, H. F. & Duncan, M. The long term dynamical behaviour of short-period comets. *Icarus* **108**, 18–36 (1994).
18. Wisdom, J. & Holman, M. Symplectic maps for the n-body problem. *Astron. J.* **102**, 1528–1538 (1991).
19. Jedicke, R. & Metcalfe, T. S. The orbital and absolute magnitude distributions of main belt asteroids. *Icarus* **131**, 245–260 (1998).
20. Fujiwara, A. *et al.* in *Asteroids II* (eds Binzel, R. P., Gehrels, T. & Matthews, M. S.) 240–265 (Univ. Arizona Press, Tucson, 1989).
21. Binzel, R. P., Bus, S. J., Burbine, T. H. & Sunshine, J. M. Spectral properties of near-earth asteroids: Evidence for sources of ordinary chondrite meteorites. *Science* **273**, 946–948 (1996).
22. 〈http://pdssbn.astro.umd.edu/SBNast/holdings/EAR-A-5-DDR-UBV-MEAN-VALUES-V1.0.html〉 (6 Feb. 2001).
23. Clark, B. E., Hapke, B., Pieters, C. & Britt, D. in *Asteroids III* (eds Bottke, W., Cellino, A., Paolicchi, P. & Binzel, R. P.) (Univ. Arizona Press, in the press).
24. Dermott, S. F., Nicholson, P. D., Burns, J. A. & Houck, J. R. Origin of the solar system dust bands discovered by IRAS. *Nature* **312**, 505–509 (1984).
25. Grogan, K., Dermott, S. F. & Durda, D. The size-frequency distribution of the zodiacal cloud: Evidence from the solar system dust bands. *Icarus* **152**, 251–267 (2001).
26. Marti, K. & Graf, T. Cosmic-ray exposure history of ordinary chondrites. *Annu. Rev. Earth Planet. Sci.* **20**, 221–243 (1992).

....

Coulomb blockade and the Kondo effect in single-atom transistors

Jiwoong Park*†‡, **Abhay N. Pasupathy***‡, **Jonas I. Goldsmith**§, **Connie Chang***, **Yuval Yaish***, **Jason R. Petta***, **Marie Rinkoski***, **James P. Sethna***, **Héctor D. Abruña**§, **Paul L. McEuen*** & **Daniel C. Ralph***

* *Laboratory of Atomic and Solid State Physics; and* § *Department of Chemistry and Chemical Biology, Cornell University, Ithaca, New York 14853, USA*
† *Department of Physics, University of California, Berkeley, California 94720, USA*
‡ *These authors contributed equally to this work*

Using molecules as electronic components is a powerful new direction in the science and technology of nanometre-scale systems[1]. Experiments to date have examined a multitude of molecules conducting in parallel[2,3], or, in some cases, transport through single molecules. The latter includes molecules probed in a two-terminal geometry using mechanically controlled break junctions[4,5] or scanning probes[6,7] as well as three-terminal single-molecule transistors made from carbon nanotubes[8], C$_{60}$ molecules[9], and conjugated molecules diluted in a less-conducting molecular layer[10]. The ultimate limit would be a device where electrons hop on to, and off from, a single atom between two contacts. Here we describe transistors incorporating a transition-metal complex designed so that electron transport occurs through well-defined charge states of a single atom. We examine two related molecules containing a Co ion bonded to polypyridyl ligands, attached to insulating tethers of different lengths. Chan-

ging the length of the insulating tether alters the coupling of the ion to the electrodes, enabling the fabrication of devices that exhibit either single-electron phenomena, such as Coulomb blockade, or the Kondo effect.

The molecules that we have investigated are depicted in Fig. 1a. They are coordination complexes in which one Co ion is bonded within an approximately octahedral environment to two terpyridinyl linker molecules with thiol end groups, which confer high adsorbability onto gold surfaces. The two molecules ([Co(tpy-$(CH_2)_5$-SH)$_2$]$^{2+}$ and [Co(tpy-SH)$_2$]$^{2+}$) differ by a five-carbon alkyl chain within the linker molecules (see Methods for details). These molecules were selected because it is known from electrochemical studies that the charge state of the Co ion can be changed from 2+ to 3+ at low energy. A cyclic voltammogram[11] for [Co(tpy-SH)$_2$]$^{2+}$ adsorbed on a gold electrode in an acetonitrile/ supporting electrolyte solution is shown in Fig. 1b, indicating that a positive voltage $V_s \approx +0.25$ V (measured against an Ag/AgCl reference) applied to the solution removes one electron from the ion. Similar results were obtained for [Co(tpy-$(CH_2)_5$-SH)$_2$]$^{2+}$ (ref. 12).

Preparation of the transistors (schematically shown in Fig. 1c) begins with the thermal growth of a 30-nm SiO$_2$ insulating layer on top of a degenerately doped Si substrate used as a back gate. Continuous gold wires with widths of less than 200 nm, lengths of 200–400 nm and thicknesses of 10–15 nm are fabricated on the SiO$_2$ layer by electron beam lithography. The wires are cleaned with acetone, methylene chloride and oxygen plasma, and placed in a dilute solution of the molecules in acetonitrile for a day or more in order to form a self-assembled monolayer on the Au electrodes. The

wires coated with molecules are then broken by electromigration, by ramping to large voltages (typically over 0.5 V) at cryogenic temperatures while monitoring the current until only a tunnelling signal is present[13]. This produces a gap about 1–2-nm-wide, across which a molecule is often found. Electrical characteristics of the molecule are determined by acquiring current versus bias voltage (I–V) curves while changing the gate voltage (V_g).

First we discuss the results obtained for the longer molecule, [Co(tpy-$(CH_2)_5$-SH)$_2$]. The measurements were performed in a dilution refrigerator with an electron temperature of less than 100 mK. In about 10% of 400 broken wires we see I–V curves as shown in Fig. 1c. The current is strongly suppressed up to some threshold voltage that depends on V_g, and then it increases in steps. In Fig. 2 we show higher-resolution colour-scale plots of the differential conductance $\partial I/\partial V$ at low bias, as a function of V and V_g for three different devices. The darkest areas on the left and right of the plots indicate the regions of no current. The bright lines located outside these regions correspond to a fine structure of current steps visible near the voltage thresholds.

This behaviour is the signature of a single-electron transistor[14], a device containing a small island which is attached to electrodes by tunnel barriers and whose charge state can be tuned using a gate voltage. In this case the island is a single Co ion. For most values of V_g, the charge state of the ion is stable at low V (dark regions). An electron does not have sufficient energy to tunnel onto the island and therefore current is blocked (Coulomb blockade). The bright lines that define the boundaries of the Coulomb-blockade regions illustrate the tunnelling thresholds for transitions between charge states. Conductance in the vicinity of $V = 0$ is allowed at a value of
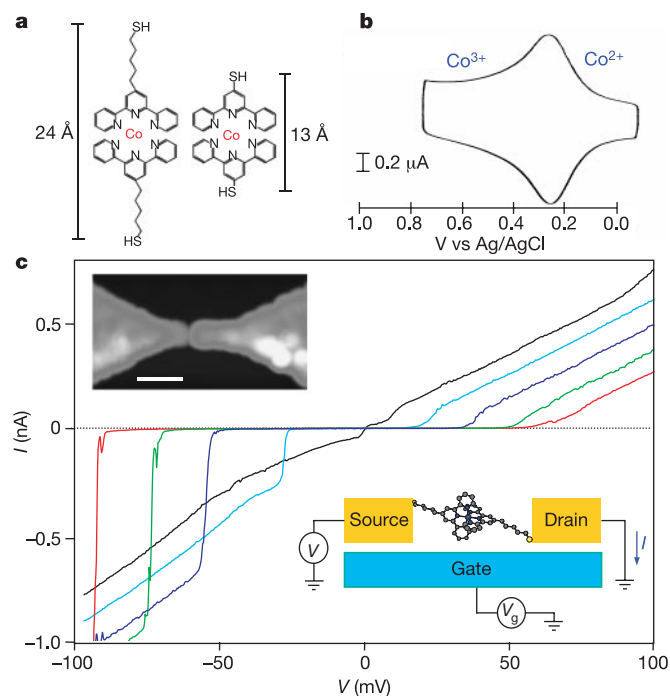

Figure 1 The molecules used in this study and their electronic properties. **a**, Structure of [Co(tpy-$(CH_2)_5$-SH)$_2$]$^{2+}$ (where tpy-$(CH_2)_5$-SH is 4′-(5-mercaptopentyl)-2,2′:6′,2″-terpyridinyl) and [Co(tpy-SH)$_2$]$^{2+}$ (where tpy-SH is 4′-(mercapto)-2,2′:6′,2″-terpyridinyl). The scale bars show the lengths of the molecules as calculated by energy minimization. **b**, Cyclic voltammogram of [Co(tpy-SH)$_2$]$^{2+}$ in 0.1 M tetra-n-butylammonium hexafluorophosphate/acetonitrile showing the Co^{2+}/Co^{3+} redox peak. **c**, I–V curves of a [Co(tpy-$(CH_2)_5$-SH)$_2$]$^{2+}$ single-electron transistor at different gate voltages (V_g) from −0.4 V (red) to −1.0 V (black) with $\Delta V_g \approx$ −0.15 V. Upper inset, a topographic atomic force microscope image of the electrodes with a gap (scale bar, 100 nm). Lower inset, a schematic diagram of the device.
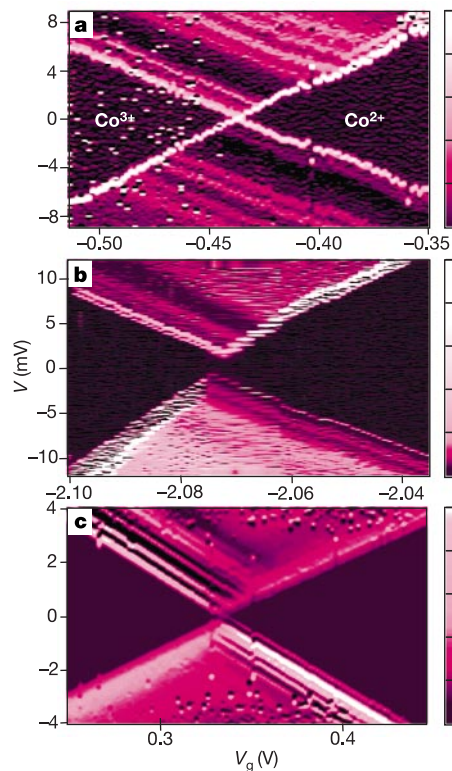
Figure 2 Colour-scale plots of differential conductance ($\partial I/\partial V$) as a function of the bias voltage (V) and the gate voltage (V_g) for three different [Co(tpy-$(CH_2)_5$-SH)$_2$] single-electron transistors at zero magnetic field. Black represents zero conductance and white the maximum conductance. The maxima of the scales are 5 nS in **a**, 10 nS in **b**, and 500 nS in **c**. The $\partial I/\partial V$ values were acquired by numerically differentiating individual I–V curves.

gate voltage V_c where the charge states are degenerate. We label the charge states as Co^{2+} and Co^{3+}, in analogy with the electrochemical measurements, and this is supported by a spin analysis presented below.

In control experiments, this behaviour has not been observed for any of 100 bare gold wires or 50 gold wires coated with tpy-$(CH_2)_5$-SH linker molecules alone without Co ions. This provides strong evidence that the island of the single-electron transistor is indeed the Co ion. We can be confident that the current near each degeneracy point is due to a single molecule because the degeneracy voltage V_c is different for each molecule owing to local variations in the electrostatic environment. The non-blockaded resistance of devices range from $100\,M\Omega$ to $\sim 1\,G\Omega$. This is comparable to the resistance recently measured for alkanedithiol molecules whose length is comparable to the linker molecule used here[7]. These results clearly illustrate that the properties of the molecule are reflected in the electrical properties of the single-electron transistor.

Additional lines in Fig. 2 running parallel to the tunnelling thresholds indicate the contributions of excited states to the tunnelling current. Lines that end in the Co^{3+} (Co^{2+}) blockade region correspond to excited levels of the Co^{3+} (Co^{2+}) charge state. The pattern of excited states is qualitatively, but not quantitatively, similar from molecule to molecule. Typically, we observe several lines at energies below 6 meV. No additional lines are resolved between about 6 and 30 meV, at which point additional strong peaks are seen.

A notable feature of the excited-state spectra is that the pattern of low-lying excitations is the same for both charge states of a given molecule. This, together with the small energy scale, suggests that the low-energy excitations are not associated with different electronic configurations. In order to test whether the excitations may be associated with the emission of a phonon[9], we have calculated the normal modes of the molecule using a quantum chemistry package (HyperChem 7.0). The simulations show normal modes with energies beginning at approximately 1 meV, with a density of ~ 2 modes per meV, in reasonable consistency with our observations. We are currently studying how the vibrational energies depend on the details of electrode attachment in order to address the differences in the excited-state spectra.

We have applied a magnetic field H to determine the magnetic state of the Co ion. Figure 3a shows a colour plot of $\partial I/\partial V$ at a magnetic field of 6 T for the same device as in Fig. 2a. A new excited Co^{2+} level, denoted by a triangle, has split from the Co^{3+} to Co^{2+} ground-state transition. The energy difference between these two states is linear in H, with a slope corresponding to a g-factor of 2.1 ± 0.2 (Fig. 3b). There is no corresponding Co^{3+} excited-state splitting from the Co^{2+} to Co^{3+} ground-state transition.

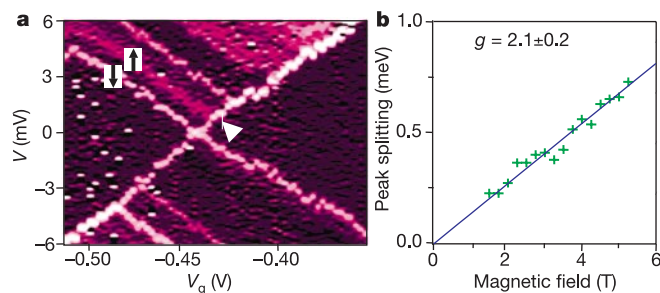These results indicate that the Co^{2+} state is spin-degenerate,

whereas the Co^{3+} state is not. An unambiguous identification of the Co^{2+} ground state as having a total spin quantum number of $S = 1/2$ and the Co^{3+} ground state as $S = 0$ is indicated by an analysis of the tunnelling current amplitudes. The lower-energy Zeeman-split state in Fig. 3a carries a current of 1.0 pA, and the second is nearly equal, 0.8 pA. Nearly equal currents are expected for $S = 0$ to $S = 1/2$ tunnelling, for a tunnelling threshold across the higher-resistance tunnel junction[15,16]. For any higher spin, the current carried by the second state would be suppressed by a Clebsch–Gordan coefficient by at least a factor of 2 compared to the first state[17].

The electronic structure inferred above is consistent with the expected electronic structure of the Co ion if its angular momentum is quenched owing to the binding to ligand molecules. A Co^{2+} ion ($3d^7$) has an odd number of electrons and possesses Kramers-degenerate states that will split in a magnetic field, whereas Co^{3+} ($3d^6$) has an even number of electrons and may have a total spin $S = 0$ so that it will not undergo Zeeman splitting[18]. Previous magnetization studies in bulk material suggest that Co^{2+} in the molecule is $S = 1/2$ at cryogenic temperatures[19]. Our measurements provide a confirmation of this result.

We now turn to the results for the shorter molecule, [Co(tpy-SH)$_2$], where we expect significantly larger conductances owing to the shorter tether length. In fact, we observe conductances that are large enough to enable us to see directly when a molecule becomes inserted in the gap between the electrodes (Fig. 4a). During the course of electromigration, the conductance initially decreases below the conductance quantum ($2e^2/h$), indicating a tunnelling gap between the electrodes. If the voltage is increased further, the current often suddenly increases by up to a factor of 10 (red dot, Fig. 4a). This behaviour is not observed for bare gold electrodes. We
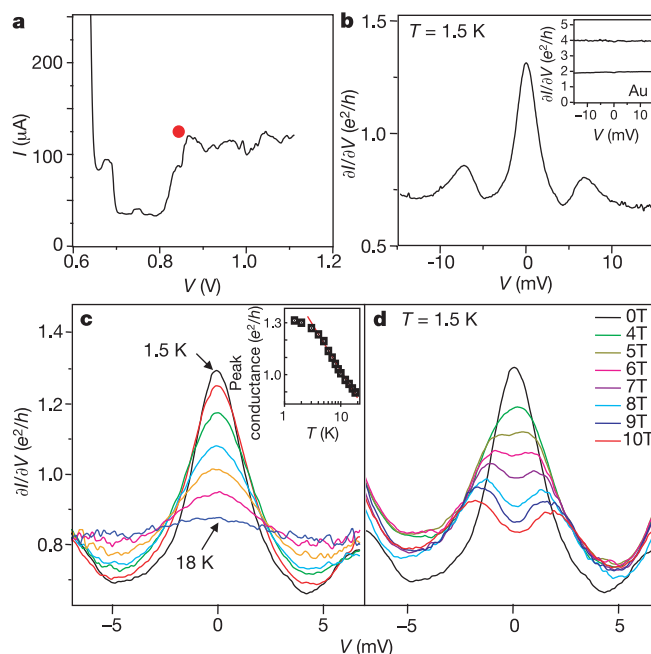
Figure 4 Devices made using the shorter molecule, [Co(tpy-SH)$_2$]$^{2+}$, exhibit the Kondo effect. **a**, Breaking trace of a gold wire with adsorbed [Co(tpy-SH)$_2$] at 1.5 K. After the wire is broken the current level suddenly increases (red dot) owing to the incorporation of a molecule in the gap. This is not seen for bare gold wires. **b**, Differential conductance of a [Co(tpy-SH)$_2$]$^{2+}$ device at 1.5 K showing a Kondo peak. The inset shows $\partial I/\partial V$ plots for bare gold point contacts for comparison. **c**, The temperature dependence of the Kondo peak for the device shown in **b**. The inset shows the $V = 0$ conductance as a function of temperature. The peak height decreases approximately logarithmically with temperature and vanishes around 20 K. **d**, Magnetic-field dependence of the Kondo peak. The peak splitting varies linearly with magnetic field.

Figure 3 Magnetic-field dependence of the tunnelling spectrum of a [Co(tpy-$(CH_2)_5$-SH)$_2$] single-electron transistor. **a**, Differential conductance plot of the device shown in Fig. 2a at a magnetic field of 6 T. There is an extra level (indicated with the triangle) owing to the Zeeman splitting of the lowest energy level of Co^{2+}. The arrows denote the spin of the tunnelling electron. **b**, Magnitude of the Zeeman splitting as a function of magnetic field.

therefore interpret the jump as the inclusion of at least one molecule in the gap between electrodes[20]. We stop the electromigration process once this happens, and study the devices at lower V.

The differential conductance $\partial I/\partial V$ for one such device is shown in Fig 4b. The most notable property is a peak in $\partial I/\partial V$ at $V = 0$. The peak has a logarithmic temperature dependence between 3 and 20 K (Fig. 4c). The peak also splits in an applied magnetic field (Fig. 4d), with a splitting equal to $2g\mu_B H$, where $g \approx 2$ and μ_B is the Bohr magneton. This peak has been clearly observed in about 30% of ~100 wires broken with the molecule, but is absent in clean gold electrodes, showing that it arises from the presence of the molecule.

The logarithmic temperature dependence and the magnetic-field splitting indicate that the peak is due to the Kondo effect[21]. The Kondo effect is the formation of a bound state between a local spin on an island and the conduction electrons in the electrodes that enhances the conductance at low biases. The observation of the Kondo effect is consistent with the identification of $S = 1/2$ for the Co^{2+} ion given above. By setting the low-temperature full-width at half-maximum of the Kondo peak equal to $2k_B T_K/e$, where T_K is the Kondo temperature[22,23], we estimate that T_K in different devices varies between 10 and 25 K. These large Kondo temperatures indicate that the coupling between the localized state and the island is strong, consistent with the high conductances found for the shorter linker molecule. In three devices the gate coupling was strong enough that T_K was increased by sweeping V_g to more negative values, indicating that the energy of the electronic state on the ion is tuned closer to the Fermi level. These devices thus provide an atomic-scale realization of the Kondo model, with Kondo temperatures higher than have been previously reported in quantum dots[24] or nanotubes[23].

We have made transistors from a single molecular complex in which one cobalt ion is connected to gold electrodes by organic barriers. By tuning the length of the organic barrier, we are able to control the coupling between the ion and the electrodes. For relatively long linker molecules, giving weak coupling, the molecule functions as a single-electron transistor. For stronger coupling, we observe Kondo-assisted tunnelling. We believe that the ability to design the electronic states of a molecular device using chemical techniques, together with the ability to measure individual molecules, will be important in molecular electronics and in the study of the physics of nanometre-scale systems. □

Methods

Synthesis of the molecules

The longer molecule investigated, $[Co(tpy-(CH_2)_5-SH)_2]^{2+}$, was synthesized from an ethanolic solution of $4'$-(5-mercaptopentyl)-$2,2':6',2''$-terpyridinyl (tpy-$(CH_2)_5$-SH) and aqueous $CoCl_2$ (ref. 12). The shorter molecule, $[Co(tpy-SH)_2]^{2+}$, was a complex of cobalt with $4'$-(mercapto)-$2,2':6',2''$-terpyridinyl (tpy-SH). The tpy-SH ligand was prepared from $4'$-chloro-$2,2':6',2''$ terpyridinyl and sodium ethanethiolate by a nucleophilic aromatic substitution followed by nucleophilic aliphatic substitution to give the thiolate anion and subsequent protonation to give the desired compound[25,26].

1. Aviram, A. & Ratner, M. A. Molecular rectifiers. *Chem. Phys. Lett.* **29**, 277–283 (1974).
2. Chen, J., Reed, M. A., Rawlett, A. M. & Tour, J. M. Large on-off ratios and negative differential resistance in a molecular electronic device. *Science* **286**, 1550–1552 (1999).
3. Collier, C. P. et al. Electronically configurable molecular-based logic gates. *Science* **285**, 391–394 (1999).
4. Reed, M. A., Zhou, C., Muller, C. J., Burgin, T. P. & Tour, J. M. Conductance of a molecular junction. *Science* **278**, 252–254 (1997).
5. Kergueris, C. et al. Electron transport through a metal-molecule-metal junction. *Phys. Rev. B* **59**, 12505–12513 (1999).
6. Bumm, L. A. et al. Are single molecular wires conducting? *Science* **271**, 1705–1707 (1996).
7. Cui, X. D. et al. Reproducible measurement of single-molecule conductivity. *Science* **294**, 571–574 (2001).
8. Dekker, C. Carbon nanotubes as molecular quantum wires. *Phys. Today* **52**, 22–28 (1999).
9. Park, H. et al. Nanomechanical oscillations in a single-C_{60} transistor. *Nature* **407**, 57–60 (2000).
10. Schön, J. H., Meng, H. & Bao, Z. Field-effect modulation of the conductance of single molecules. *Science* **294**, 2138–2140 (2001).
11. Bard, A. J. & Faulkner, L. R. *Electrochemical Methods: Fundamentals and Applications* (Wiley & Sons, New York, 2001).
12. Maskus, M. & Abruna, H. D. Synthesis and characterization of redox-active metal complexes sequentially self-assembled onto gold electrodes via a new thiol-terpyridine ligand. *Langmuir* **12**, 4455–4462 (1996).
13. Park, H., Lim, A. K. L., Park, J., Alivisatos, A. P. & McEuen, P. L. Fabrication of metallic electrodes with nanometer separation by electromigration. *Appl. Phys. Lett.* **75**, 301–303 (1999).
14. Grabert, H. & Devoret, M. H. *Single Charge Tunneling: Coulomb Blockade Phenomena in Nanostructures* (Plenum, New York, 1992).
15. Deshmukh, M. M., Bonet, E., Pasupathy, A. N. & Ralph, D. C. Equilibrium and nonequilibrium electron tunneling via discrete quantum states. *Phys. Rev. B* **65**, 073301-1–073301-4 (2002).
16. Bonet, E., Deshmukh, M. M. & Ralph, D. C. Solving rate equations for electron tunneling via discrete quantum states. *Phys. Rev. B* **65**, 045317-1–045317-10 (2002).
17. Akera, H. Coulomb staircase and total spin in quantum dots. *Phys. Rev. B* **60**, 10683–10686 (1999).
18. Ralph, D. C., Black, C. T. & Tinkham, M. Gate-voltage studies of discrete electronic states in aluminum nanoparticles. *Phys. Rev. Lett.* **78**, 4087–4090 (1997).
19. Oshio, H., Spiering, H., Ksenofontov, V., Renz, F. & Guetlich, P. Electronic relaxation phenomena following $^{57}Co(EC)^{57}Fe$ nuclear decay in $[Mn^{II}(terpy)_2](ClO_4)_2.1/2H_2O$ and in the spin crossover complexes $[Co^{II}(terpy)_2]X_2.nH_2O$ (X = Cl and ClO$_4$): A Moessbauer emission spectroscopic study. *Inorg. Chem.* **40**, 1143–1150 (2001).
20. Bezryadin, A., Dekker, C. & Schmid, G. Electrostatic trapping of single conducting nanoparticles between nanoelectrodes. *Appl. Phys. Lett.* **71**, 1273–1275 (1999).
21. Wolf, E. L. *Principles of Electron Tunneling Spectroscopy* Ch. 8 (Oxford Univ. Press, Oxford, 1989).
22. van der Wiel, W. G. et al. The Kondo effect in the unitary limit. *Science* **289**, 2105–2108 (2000).
23. Nygård, J., Cobden, D. H. & Lindelof, P. E. Kondo physics in carbon nanotubes. *Nature* **408**, 342–346 (2000).
24. Goldhaber-Gordon, D. et al. Kondo effect in a single-electron transistor. *Nature* **391**, 156–159 (1998).
25. Testaferri, L., Tiecco, M., Tingoli, M., Chianelli, D. & Montanucci, M. Simple syntheses of aryl alkyl thioethers and of aromatic thiols from unactivated aryl halides and efficient methods for selective dealkylation of aryl alkyl ethers and thioethers. *Synthesis (Stuttgart)* **9**, 751–755 (1983).
26. Mathis, J. M. & Pallenberg, A. J. Preparation of novel, functionalized 1,10-phenanthrolines. *Synth. Commun.* **27**, 2943–2951 (1997).

Competing interests statement

The authors declare that they have no competing financial interests.

Correspondence and requests for materials should be addressed to P.M. (e-mail: mceuen@ccmr.cornell.edu) or D.R. (e-mail: ralph@ccmr.cornell.edu).

••

Kondo resonance in a single-molecule transistor

Wenjie Liang*, Matthew P. Shores†, Marc Bockrath*, Jeffrey R. Long† & Hongkun Park*

* *Department of Chemistry and Chemical Biology, Harvard University, 12 Oxford Street, Cambridge, Massachusetts 02138, USA*
† *Department of Chemistry, University of California, Berkeley, California 94720, USA*

When an individual molecule[1], nanocrystal[2–4], nanotube[5,6] or lithographically defined quantum dot[7] is attached to metallic electrodes via tunnel barriers, electron transport is dominated by single-electron charging and energy-level quantization[8]. As the coupling to the electrodes increases, higher-order tunnelling and correlated electron motion give rise to new phenomena[9–19], including the Kondo resonance[10–16]. To date, all of the studies of Kondo phenomena in quantum dots have been performed on systems where precise control over the spin degrees of freedom is difficult. Molecules incorporating transition-metal atoms provide powerful new systems in this regard, because the spin and orbital degrees of freedom can be controlled through well-defined chemistry[20,21]. Here we report the observation of the Kondo effect in single-molecule transistors, where an individual divanadium molecule[20] serves as a spin impurity. We find that the